Frictional dynamics of viscoelastic solids driven on a rough surface

François P. Landes*
The Abdus Salam International Center for Theoretical Physics, Strada Costiera 11, 34014 Trieste, Italy and Laboratoire de Physique Théorique et Modèles Statistiques (UMR CNRS 8626), Université Paris-Sud, Orsay, France

Alberto Rosso
Laboratoire de Physique Théorique et Modèles Statistiques (UMR CNRS 8626), Université Paris-Sud, Orsay, France

E. A. Jagla
Centro Atómico Bariloche and Instituto Balseiro (UNCu), Comisión Nacional de Energía Atómica, (8400) Bariloche, Argentina
(Received 31 March 2015; published 16 July 2015)

We study the effect of viscoelastic dynamics on the frictional properties of a (mean-field) spring-block system pulled on a rough surface by an external drive. When the drive moves at constant velocity V, two dynamical regimes are observed: at fast driving, above a critical threshold V^c, the system slides at the drive velocity and displays a friction force with *velocity weakening*. Below V^c the steady sliding becomes unstable and a stick-slip regime sets in. In the slide-hold-slide driving protocol, a peak of the friction force appears after the hold time and its amplitude increases with the hold duration. These observations are consistent with the frictional force encoded phenomenologically in the rate-and-state equations. Our model gives a microscopical basis for such macroscopic description.

DOI: 10.1103/PhysRevE.92.012407 PACS number(s): 62.20.Qp, 05.10.Gg, 46.55.+d

I. INTRODUCTION

Friction is behind many phenomena of our every day life experience such as the adhesion of car tires on the road [1,2], the sound emitted by a violin [3,4], or the wear of human articular joints [5]. Often, in these situations, the two bodies in contact may display discontinuous dynamics, the so-called stick-slip dynamics [6,7], in which periods of rapid movement (slip) are followed by periods of relative rest (stick). At the macroscopic scale the stick-slip motion is justified by the empirical difference observed between the static and dynamic friction coefficient, but a general explanation of this phenomenon from first principles is not yet available. The introduction of viscoelastic effects in the dynamics can be the key for a microscopic theory of friction. In fact, we have recently shown that viscoelastic solids sliding on a rough substrate can display a stick-slip instability [8]. Interestingly it was also pointed out that viscoelasticity is at the origin of the observed precursors, the microslips occurring at the onset of slip [9–11].

A scheme of the model studied in Ref. [8] is reproduced for convenience in Fig. 1. It consists of an ensemble of interacting blocks driven at velocity V on a rough substrate. The macroscopic friction arises from the real area of solid-substrate contact, which consists in the junctions between asperities. When the block is stuck on the rough substrate, the elastic energy of the spring k_0 slowly accumulates over time and is released when junctions break, letting the block move. The rupture of a single junction can trigger further rupture, with a characteristic time τ_0 that characterizes the dynamics of the block-substrate contact. In the quasistatic limit ($V \to 0^+$), when the driving time scale τ_D is very slow compared to τ_0, the chain of events triggered by a single rupture can be very large and is called an *avalanche*.

In the case of purely elastic interactions between the blocks, the macroscopic friction force, namely the average elongation of the spring k_0, is the control parameter of the depinning transition, a second-order transition between a pinned phase and a phase where the system slides at the driving velocity V [12–16]. Viscoelastic interactions [17] change the nature of the moving phase, inducing hysteretic behavior, as it was shown by Marchetti *et al.* [18,19] in the context of the plastic depinning transition of a vortex lattice.

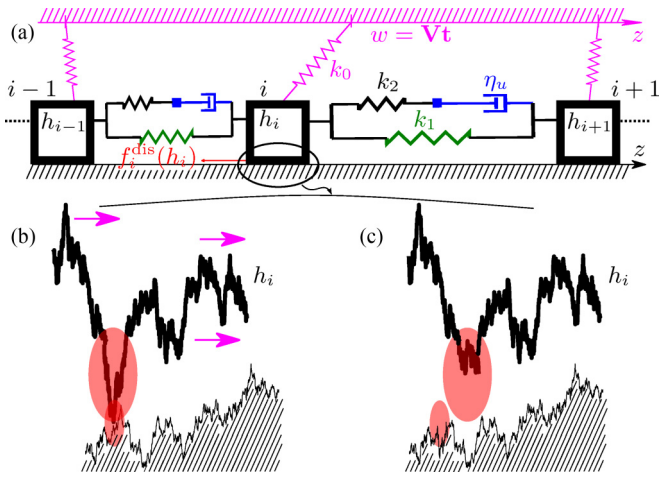

FIG. 1. (Color online) Sketch of the viscoelastic interface model. (a) The interface consists in blocks (labeled $i, i+1, \ldots$) located at the positions $h_i, h_{i+1}, \ldots$ (empty squares) and bound together via a combination of springs (k_1,k_2) and dashpots (η_u). Driving is performed via springs k_0 linked to the position $w = Vt$. (b, c) The asperities that provide the contact (highlighted with ellipses) hinder the sliding of the block on its substrate, with a random force $f_i^{\rm dis}(h_i)$ acting as a microscopic static friction force. (c) The solid sled on the substrate and the asperities under stress are changed.

*francois.landes@gmail.com

In the quasistatic driving limit ($\tau_0 \ll \tau_D$), the presence of viscoelasticity (with a characteristic time τ_u) has been shown to produce a rich phenomenology of the avalanche dynamics, with main shocks, aftershocks, and spatiotemporal correlations similar to that observed in seismology [8,20–24]. When the viscoelastic relaxation is very fast compared to the driving ($\tau_u \ll \tau_D$), these system-size avalanches can be understood as a stick-slip dynamics of the mean-field model [8].

In the present paper we study the case where the driving rate τ_D is of the same order of magnitude as the viscoelastic time scale τ_u, but is still very slow compared to the duration of each single avalanche: $\tau_0 \ll \tau_u \simeq \tau_D$. We show that in this limit, the system displays the basic features of dry friction. In particular, when a uniform driving is applied, we observe a transition between a stick-slip regime (slow driving, $\tau_u \ll \tau_D$) and a steady-sliding regime (fast driving, $\tau_u \gg \tau_D$). When the driving velocity is not constant, as in the case of the slide-hold-slide protocol, our results display qualitatively the kind of behavior observed in the experiments [25], most remarkably, the existence of a peak in the friction force after the hold period, which becomes larger as the hold time increases. It must be noted that this kind of experiments on friction dynamics are usually modeled using the so-called rate-and-state equations [26,27], which incorporate the fact that the friction force does not simply depend on the relative velocity between the two nominal surfaces but also depends on the history of the contact, via a macroscopic "state" variable θ. In our model this dependence is encoded in the state of the microscopic viscoelastic elements. In this way our model gives a microscopical basis for the rate-and-state description of friction.

The paper is organized as follows. In Sec. II we briefly present the model. In Sec. III we study the case of uniform driving, and we complete this study with the slide-hold-slide protocol in Sec. IV. We then interpret our results in terms of rate-and-state formalism in Sec. V and conclude in Sec. VI.

II. MODEL

The equations of motion for the model pictured in Fig. 1 are derived in Appendix A:

$$\eta_0 \partial_t h_i = k_0(w - h_i) + k_1 \nabla^2 h_i + f_i^{\mathrm{dis}}(h_i) + k_2 \nabla^2 h_i - k_2 u_i, \tag{1}$$

$$\eta_u \partial_t u_i = k_2 \nabla^2 h_i - k_2 u_i. \tag{2}$$

Here h_i is the position of the block i, $w = Vt$ is the driving term in the uniform driving protocol, and η_0 is the damping coefficient for the sliding of blocks relatively to the substrate. The internal variable u_i accounts for the dashpots elongation, which induce the damping of the elastic force, $k_2(\nabla^2 h_i - u_i)$, acting on the block i. The characteristic response time of blocks is $\tau_0 = \eta_0/\max(k_0, k_1, k_2)$, while the characteristic readjustment time for the dashpots is $\tau_u = \eta_u/k_2$.

The random force $f_i^{\mathrm{dis}}(h_i)$ mimics the contacts between the asperities of the block and those of the surface and acts as a microscopic static friction force. When a contact is broken, two things happen: (i) the block moves and redistributes stress to neighboring blocks, and (ii) the asperities involved in the junction are renewed, as sketched in Fig. 1(c). This renewal process makes the asperity landscapes different for each block.

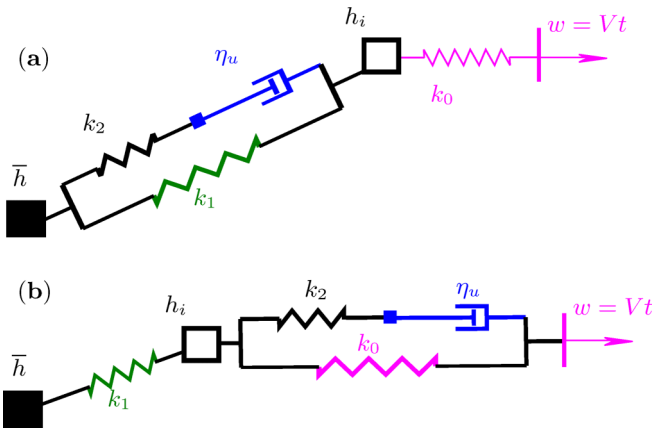

FIG. 2. (Color online) (a) Mean-field model of Eqs. (1) and (2). (b) Equivalent model if the solution is stationary.

For simplicity, we consider that the random force $f_i^{\mathrm{dis}}(h_i)$ acting on block i is completely independent from that acting on other blocks.

Equations (1) and (2) were introduced in Ref. [8] and studied in $d = 2$ and in mean field for $V = 0^+$. Here we extend the mean-field approximation [which corresponds to replace the laplacian $\nabla^2 h_i$ with $\overline{h} - h_i$, where $\overline{h}$ is the average location of the blocks; see Fig. 2(a)] to the finite velocity case. Note that this model couples the h_i's with $\overline{h} \equiv \sum_i h_i/N$; i.e., it actually represents N times the k_2, η_u, k_1 units. As it is usual in the mean-field case, the values of the parameters are thus scaled as $k_2/N, \eta_u/N, k_1/N$, to ensure the extensive character of the total energy. We compute the macroscopic friction force

$$\sigma \equiv k_0(w - \overline{h}), \tag{3}$$

accumulated in the system for different driving protocols and adopt the so-called "narrow wells" approximation [13]. In this scheme, the disorder $f_i^{\mathrm{dis}}(h_i)$ is modeled as a collection of narrow pinning wells representing impurities, with spacings z distributed as $g(z)$ and with average $\overline{z} = \int_0^\infty z g(z) dz$. As the wells are very narrow, the disorder force $f_i^{\mathrm{th}}(h_i)$ that derives from this potential is 0 everywhere except for countably many points. Within this approximation each block is pinned in a single narrow well (see Fig. 9 in Appendix A). For simplicity we consider narrow wells of constant depth (and shape), namely, the random thresholds are constant, $f_i^{\mathrm{th}} = \mathrm{const.} = 1$.

Our model provides a description of the interface between two solid surfaces where all dynamical properties are concentrated in one of them, and the other (the substrate) is taken as inert. It has to be emphasized that the blocks have to be considered as microscopic single contacts between the surfaces, and as such they are individually given a rather trivial and time-independent interaction law with the substrate. In addition, the k_1, k_2, and η_u elements (and to a certain extent also the k_0 springs) must be considered as part of the surface itself, the whole picture in Fig. 2 thus representing a small part of the two solid surfaces in contact.

Note that here and in the rest of the paper, we give all quantities in dimensionless form. In order to restore physical units we need to reintroduce the units of the fundamental quantities: distance along the h direction ($\mathbf{z}$), along the surface

(**x**), force (**f**), and time (**t**), so for instance the previous unit value of $f^{\rm th}$ means $f^{\rm th} = 1\mathbf{f}$, spring constants k_1,k_2 are given in units of $\mathbf{fx}^2/\mathbf{z}$, k_0 is in units of $\mathbf{f}/\mathbf{z}$, etc.

III. UNIFORM DRIVING PROTOCOL

At long times, under a driving performed at constant velocity V, the solution of Eqs. (1) and (2) becomes independent of the initial condition and, in mean field, two phases are observed: for small V we find a limit cycle solution that corresponds to a stick-slip phase, whereas for large V a stationary solution exists. The stationary value of the friction force, $\sigma(V)$, can be computed analytically for $g(z) = \delta(z - \bar{z})$ using the crucial remark that if a steady sliding regime exists then in this regime $\bar{h}$ moves with velocity V. In particular, $\bar{h} = Vt - \sigma(V)/k_0$. In the stationary regime the k_2-plus-dashpot branch shown in Fig. 2(a) can also be thought of as connecting h_i with $w = Vt$, instead of $\bar{h}$, as indicated in Fig. 2(b). This is so because the additional stretching induced by the time-independent shift, $w - \bar{h} = \sigma(V)/k_0$, is quickly absorbed by the dashpot, without altering the forces in any manner.

The model in Fig. 2(b) coincides with the one studied by Dobrinevski, Le Doussal, and Wiese in Ref. [28] and can be solved exactly. In particular the friction force writes (see Appendix C)

$$\sigma(V) = f^{\rm th} - \left[V\eta_u - \frac{\bar{z}k_2}{e^{\bar{z}k_2/V\eta_u} - 1} \right] - \frac{\bar{z}}{2}(k_0 + k_1), \quad (4)$$

and it is bounded by the two limiting values

$$\sigma(V \to 0) = f^{\rm th} - \frac{\bar{z}}{2}(k_0 + k_1), \quad (5)$$

$$\sigma(V \to \infty) = f^{\rm th} - \frac{\bar{z}}{2}(k_0 + k_1 + k_2). \quad (6)$$

Note that:

(1) The friction force decreases as the driving velocity increases, an effect called *velocity weakening*, and observed in tribology experiments for different materials, especially at very low velocities [25,29].

(2) The velocity weakening displays a characteristic $1/V$ decay at large V.

(3) The dependence on k_0 and k_1 is limited to the last term in Eq. (4), which accounts for a constant shift of the whole $\sigma(V)$ curve.

Velocity weakening is a necessary link between the static ($V = 0$) and kinetic ($V > 0$) friction coefficients, and as such is known to be crucial in the triggering of instabilities in sliding systems, leading to stick-slip motion [6] and to the existence of earthquakes in sliding tectonic faults [30]. For a review on nanoscale models of friction and experimental results on nanotribology one should consult Ref. [31] or the letter [32], which contains accessible references to the literature. In our model, velocity weakening is a direct consequence of the viscoelastic relaxation. In fact, the model without viscoelasticity lacks any velocity dependence of the friction force, as in that case there is no internal time scale to compete with the driving time scale. It should be noted that the most commonly observed velocity-weakening friction law is only logarithmic in V but cannot be expected here because we

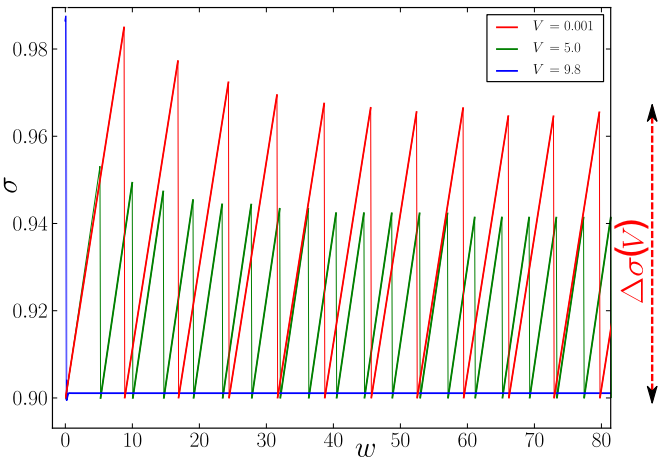

FIG. 3. (Color online) Evolution of the stress σ over time for three velocities. At slow driving, $V = 0.001$ (large amplitude), $V = 5$ (small amplitude), the stress oscillates periodically, with an amplitude that we denote $\Delta\sigma(V)$. At faster driving, $V = 9.8$ (lower curve, almost always constant), the stress reaches a stationary value after a very short transient. The precise choice of initial condition only impacts the transient regimes. We used $k_0 = 0.01, k_1 = 0.1, k_2 = 0.9$, and $\bar{z} = 0.1$.

introduced a single relaxation time scale in a mean-field model. This echoes the results found in Ref. [33], where a $1/V$ velocity-weakening law is found to occur in a noninteracting block model with random friction coefficients, where the relaxation time scale is present thanks to the noninstantaneous slips. One may also note that we do not expect any of the velocity-strengthening scenarios (as those proposed in Ref. [34]) to occur either, since we do not account for any of the faster mechanisms that become relevant under fast driving.

We now turn on the numerical study of the mean-field version of Eqs. (1) and (2) using an uncorrelated distribution of pinning wells, with mean $\bar{z}$, namely $g(z) = \bar{z}^{-1}e^{-z/\bar{z}}$. In practice we implement the Fokker-Planck method used in Ref. [8], adapted to the case of finite driving velocity. All technical details are left to Appendix B.

In Fig. 3, the evolution of the stress over time is compared for three values of the velocity: at slow driving velocities the stress $\sigma(t)$ oscillates periodically with an amplitude denoted $\Delta\sigma(V)$, while at fast driving a stationary value is reached [i.e., $\Delta\sigma(V) = 0$]. Note that the amplitude $\Delta\sigma(V)$ of the oscillations is also the width of the stress drops or "gaps" that occur during the system-size events.

This behavior points to a bifurcation of the dynamics as velocity is reduced. To study this effect, we report in Fig. 4 the maximum and minimum of the friction force over time, as a function of the driving velocity V, for various values of k_0. We observe that the stress gap vanishes smoothly at the transition point $V = V^c$, pointing to a "second-order" dynamical phase transition in the order parameter $\Delta\sigma$. In Fig. 5 we show the full phase diagram of the system in the k_0-V plane. There, for various sets of (k_1, k_2) we observe a divergence of V^c as $1/k_0$. This $1/k_0$ dependence at low k_0 comes directly from the uniform increase of the pulling force as $k_0 Vt$ and implies that for any non zero values of k_1, k_2, and V, there will always be

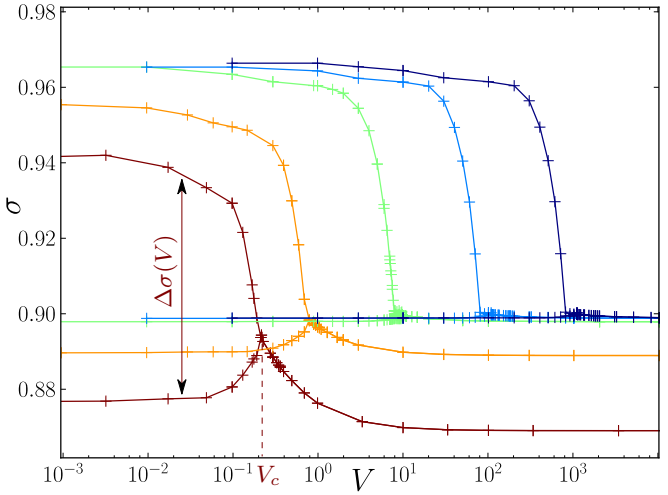

FIG. 4. (Color online) Friction force against driving velocity, for different values of k_0 ($k_0 = 0.3, 0.1, 0.01, 0.001, 0.0001$, from left to right); and constant $k_1 = 0.1$, $k_2 = 0.9$, $\bar{z} = 0.1$. In the slow driving regime (on the left), motion occurs mostly through the abrupt slips during which stress falls from the stress before slip, σ_B (up), to the stress after slip, σ_A (down). In the faster driving regime, the dynamics is stationary and friction decreases with velocity. Crosses indicate the values of V for which the numerical integration has actually been performed.

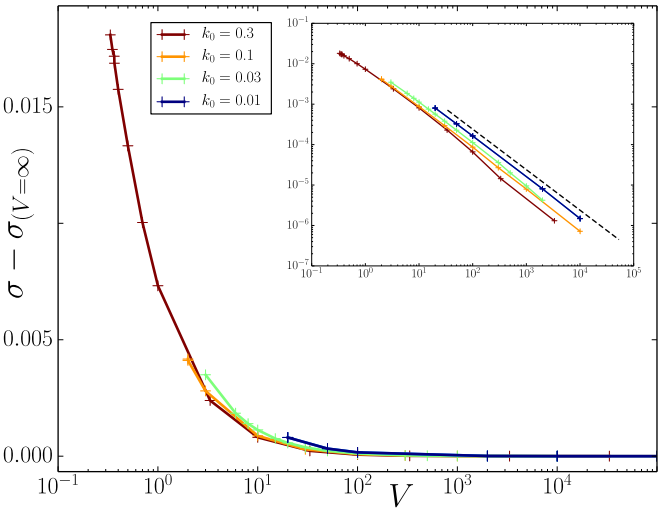

FIG. 6. (Color online) Velocity weakening in the steady-slip regime ($V > V^c$), far from the critical point. We observe that σ decreases when the velocity increases. For $V \to \infty$, the decay in the friction force toward the limiting large-velocity value $\sigma_{V=\infty}$ goes as $\sim V^{-1}$. Inset: plot in the log-log coordinates. The dashed line gives the pure power law with exponent -1. We used the same color code as in previous figures (curves that go to larger values are the lower k_0's).

a value of k_0 below which some stick-slip dynamics occurs, even at very large velocities.

In the stationary regime, our simulations confirm, overall, the friction behavior of Eq. (4). In particular, in Fig. 6 we observe a clear velocity weakening with a characteristic $1/V$ decay toward $\sigma(V \to \infty) = 1 - (k_0 + k_1 + k_2)\bar{z}/2$.

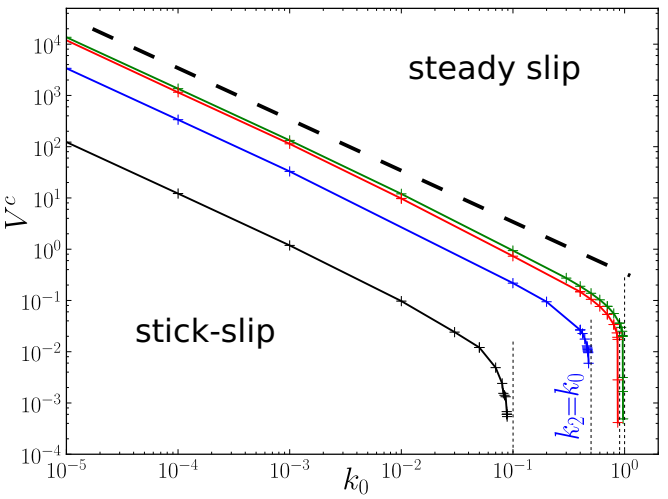

FIG. 5. (Color online) Phase diagram in the k_0-V plane, for different sets of (k_1,k_2) values: from bottom to top we used $(k_1 = 0.0, k_2 = 1.0)$, $(0.1, 0.9)$, $(0.5, 0.5)$, $(0.9, 0.1)$. In the lower-left region, the system behaves in a nonstationary way; i.e., we have stick-slip motion. For $k_0 \geqslant k_2$, the system is never nonstationary, even at quasistatic driving, as predicted in Ref. [35]. The bold dashed line has slope one, indicating a scaling of the critical velocity as $V^c \sim k_0^{-1}$ for small k_0's. The thin dashed vertical lines indicate the asymptotic behavior $V^c \to 0$ when $k_0 \to k_2^-$.

IV. SLIDE-HOLD-SLIDE PROTOCOL

Slide-hold-slide experiments are an important tool in the investigation of the tribology of solids. When the sliding of a solid is interrupted for some time Δt, the contacts at the surface of the solid can strengthen over time, so that when sliding is resumed, a peak in the friction force has to be overcome before one recovers the stationary friction force. The amplitude of the friction peak increases with the hold time Δt since the relaxation is more effective when it has more time to act. Our model has all the necessary ingredients to reproduce the peak in the friction force after a hold period. In fact, when driven at a finite velocity, the viscoelastic elements do not have the time to completely relax to the most convenient (i.e., lowest energy) configuration at each global position. If a hold time is given to the system, the mechanical energy reduces as the viscoelastic elements relax. Upon resuming driving, this lower-energy configuration requires a larger stress to initiate motion again. Thus the effect is expected to become stronger as the hold time increases, saturating at hold times much larger than the viscoelastic relaxation time.

To simulate this process, we set the driving velocity V to a value at which a steady sliding is observed. Once we reached a stationary dynamics, the driving is stopped for some time interval Δt and then resumed. The evolution of the friction force during this protocol in our model is shown in Fig. 7 (left). The height of the friction peak as a function of the hold time Δt is shown in Fig. 7 (right).

We observe some similarities and some differences when comparing our results with experimental observations. In

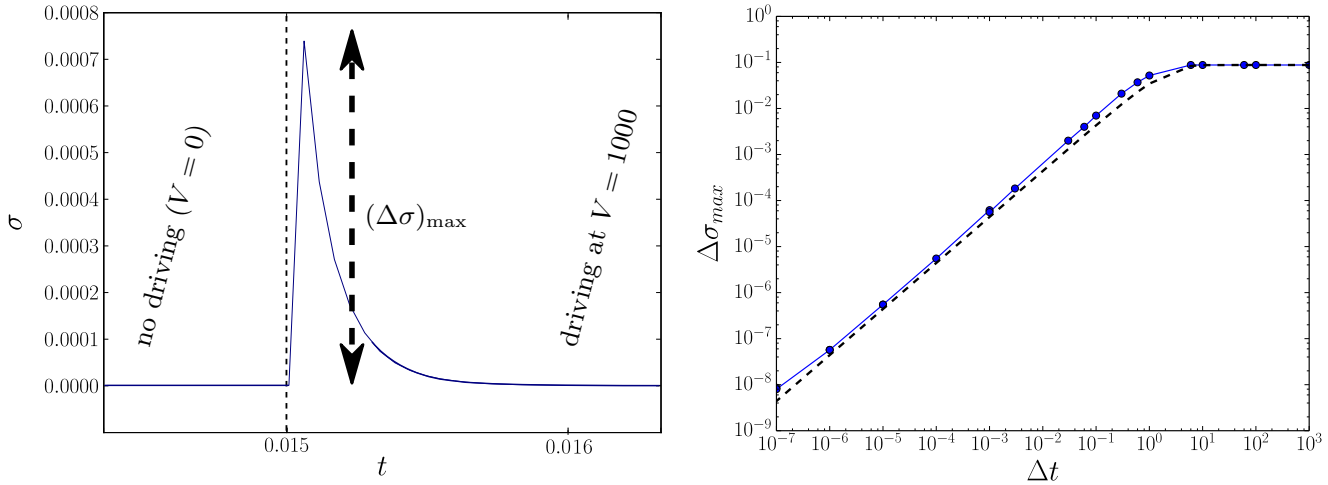

FIG. 7. (Color online) Slide-hold-slide experiment. Left: Evolution of the stress σ over time under this protocol, around the time when driving is resumed ($t = 0.015$ here). The driving velocity is $V = 1000$. Right: For many different hold times Δt, we record the maximal deviation $(\Delta\sigma)_{\max}$ from stationary stress (blue points). This deviation corresponds to the gap between static and kinetic friction coefficient. In our model we observe a linear growth of the gap with Δt while in experiments a logarithmic increase is measured. The dashed line gives the purely exponential saturation: $\Delta\sigma_{\max} = \Delta\sigma_\infty(1 - e^{-\Delta t/\tau})$, with $\tau = 2$ and $\Delta\sigma_\infty \equiv \Delta\sigma_{\max}(\Delta t = \infty)$.

experiments, during the hold time the stress shows a relaxation toward some lower value, something that is not observed in our model. The reason is that stress relaxation can occur only if some secondary avalanches (aftershocks) are triggered by the viscoelastic relaxation. When the pinning thresholds f^{th} have a single value, then aftershocks are excluded and the decrease cannot happen. However, in models with a wide distribution of pinning thresholds this relaxation has been observed [20] and is compatible with experiments.

Qualitatively, the friction peak is similar in our simulations and in experiments: in both cases its height increases as a function of the hold time, but in experiments the increase is usually reported to be logarithmic, while here we observe an exponential saturation at large Δt. The reason for this difference is that our model contains only a single relaxation time constant, which naturally defines a typical time scale, above which the system is fully relaxed and thus no longer evolves.

V. ANALYSIS IN TERMS OF RATE-AND-STATE EQUATIONS

It has been long realized that the friction force cannot be described by a single valued function of the instantaneous velocity. The history of the contact plays an important role in determining the actual friction force. Our model is an example of such a case, since the value of the friction force depends on the state of the viscoelastic elements, which in turn depend on the history of the system. We thus briefly recall the standard rate and state formalism, and then show how it provides an appropriate framework to understand our results.

A. The RS formalism

Phenomenologically, the behavior of frictional contacts has been successfully described through the formalism named rate-and-state (RS) friction, originated in the works of Dieterich and Ruina [26,27]. Instead of assuming that there exists only a kinetic and a static friction coefficient, the RS formalism assumes that the friction coefficient continuously depends on the relative velocity v between the two surfaces (the rate variable) and on a state variable usually called θ. We recall that by definition, the friction coefficient μ acts as a threshold for the friction force σ actually arising from the contacts: we always have $\sigma \leqslant \mu F_N$, where F_N is the force normally applied on the solid. The usual RS form for $\mu(v,\theta)$ is

$$\mu(v,\theta) = \mu_0 + a\log(v) + b\log(\theta/D_c), \tag{7}$$

where a, b are positive constants. Note that we use a small v to indicate the instantaneous velocity, which may differ from the driving velocity V. The a term describes the so-called "direct effect," the increase of friction with increase of the relative velocity commonly observed in many materials.

The state variable θ is supposed to follow a second equation, usually written

$$\dot\theta = 1 - \frac{\theta v}{D_c}, \tag{8}$$

where D_c is the "critical slip distance," i.e., the amount of slip (of the center of mass of the sliding block) necessary to break a newly formed junction.

Under steady sliding, we have $\dot\theta = 0$, $\theta = D_c/v$, and the RS Eqs. (7) and (8) simplify into

$$\mu(v,\theta) = \mu_0 + (a-b)\log(v). \tag{9}$$

If $b > a$ this equation describes the phenomenon of velocity weakening, namely a reduction of the friction coefficient when velocity increases. Velocity weakening is a crucial ingredient involved in the description of seismic phenomena [30]. In the case in which the contact is at rest ($v = 0$), we get $\dot\theta = 1$, i.e., $\theta(t) = \theta_0 + t$, and according to Eq. (7) we obtain an increase of the static friction coefficient with the time of contact. RS equations have been used to describe the behaviors of frictional systems under a variety of nonsteady sliding conditions, providing an excellent phenomenological description for numerous systems.

B. Interpretation of our model in terms of RS equations

Under uniform driving, our model displays two features that are common to many frictional systems: a velocity-weakening friction law and a bifurcation to a stick-slip regime for low driving velocities. We have described in Sec. III how the velocity-weakening effect appears in the model. Now we will see that assuming the existence of this effect, the bifurcation to a stick-slip regime at low velocities is captured in all its detail by the use of the RS formalism.

The usually assumed form Eq. (9) of the friction coefficient is not appropriate to accurately describe the results observed in our model in the steady sliding regime. On the one hand, our model does not have any ingredient that could produce a direct effect in the RS Eq. (7), suggesting that we should use $a = 0$. On the other hand, the logarithmic b term is not appropriate in our case, mainly because we have considered only a relaxation mechanism that is described by a single time constant, the one associated to the dashpot and k_2 springs. Instead, from our simulations of Sec. III (as for instance those in the right part of Fig. 4) we can construct a simple analytical expression for the friction coefficient in the steady sliding regime:

$$\mu^{\text{steady}} \simeq f^{\text{th}} - \frac{\bar{z}}{2}(k_0 + k_1 + k_2) + \frac{0.007}{v + 0.078}, \qquad (10)$$

where the numerical values correspond to $k_1 = 0.1$, $k_2 = 0.9$, and $\bar{z} = 0.1$. We remark that this is just a simple, although accurate fitting to the numerical results that allows the analytical treatment presented below, but it has no additional particular significance.

We now assume that under any nonsteady-sliding situation, the value of the friction coefficient can still be written in terms of the function found in the steady state. Using the fact that in the steady state $v \equiv D_c/\theta$, we write

$$\mu(\theta) = f^{\text{th}} - \frac{\bar{z}}{2}(k_0 + k_1 + k_2) + \frac{0.007}{D_c/\theta + 0.078}. \qquad (11)$$

The time evolution of θ will be assumed to be described by the standard RS evolution, Eq. (8). The sliding contact is coupled to a driving spring pulled at constant velocity V, so that the pulling force reads

$$\sigma = (Vt - x)k_0, \qquad (12)$$

where x is the spatial average coordinate of the contact, i.e., $\dot{x} = v$. This force σ is also the actual instantaneous friction force arising from the contacts. Our aim is now to determine the temporal evolution of x and σ and reproduce the bifurcation behavior that we obtained in Sec. III.

If steady sliding is assumed, the force μF_N must balance the pulling force, and we get $\theta = D_c/V$, $v = V$. However, steady sliding may be unstable due to the following process: if at some moment x is stopped, the pulling force starts to increase according to $\sigma = \sigma^0 + Vtk_0$. On the other hand, the friction force starts to increase due to the increasing of θ, according to $\mu = \mu(\theta_0 + t)$. If the initial increase of μF_N is more rapid than the increase of σ, the contact will stay stuck as long as $\mu F_N > \sigma$, until eventually the pulling force becomes larger than the pinning force, and a rapid slip moves the value of x to a new position. If $\mu F_N < \sigma$, slip occurs and is essentially instantaneous since we have not added inertia to the contact. During the slip stage, the value of θ is reduced following Eq. (8), which in the rapid slip limit can be written as $d\theta = -\theta dx/D_c$ and analytically integrated. Slip finishes when σ drops below μF_N again, and a new stick-slip cycle begins. We have integrated Eqs. (11), (8), and (12) and in fact obtained steady sliding for large V, and a stick-slip behavior at small V, in which the value of σ oscillates between two values, $\sigma_{\max}$ and $\sigma_{\min}$. In Fig. 8 we plot the values of $\sigma_{\max}$ and $\sigma_{\min}$ (or the single value σ in case of steady sliding) as a function of V for the same set of k_0 values used in Fig. 4. It can be seen that the value of D_c enters in the problem only in combination with the spring stiffness, as kD_c. In Fig. 8 we used $D_c = 0.06$ to achieve the best fitting with the results of Fig. 4. We note that as suggested by its original meaning, D_c is of the order of $\bar{z}$, which is the distance at which the correlations between pinning forces disappears. In addition to the coincidence of the two figures in the steady-sliding regime [which is enforced by hand through the choice of the μ^{steady} function in Eq. (10)], we see that the RS formalism gives a very good coincidence in the low-velocity, stick-slip regime.

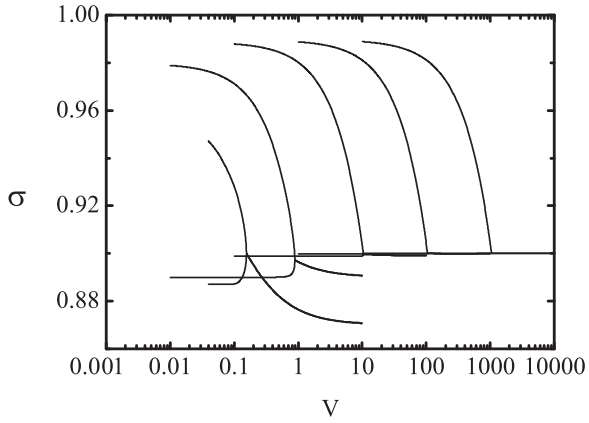

FIG. 8. Friction force as a function of velocity for the same set of values as described in the caption of Fig. 4, using the RS formalism. The form of the steady-sliding part of the curves is introduced by hand. We used a value $D_c = 0.06$ to achieve the best fitting. The RS formalism yields the form of $\sigma_{\max}$ and $\sigma_{\min}$ for $V < V^c$.

A careful analysis of our RS equations near the bifurcation point shows that the two values $\sigma_{\max}$ and $\sigma_{\min}$ depart symmetrically from the branch of steady sliding and are such that $\sigma_{\max} - \sigma_{\min} \sim (V^c - V)^{1/2}$, which corresponds to a Hopf bifurcation. Note, however, that the validity range of these scalings becomes progressively smaller as k_0 is reduced, and in the $k_0 \to 0$ limit we get the scaling $\sigma_{\min} \sim$ const, $\sigma_{\max} - \sigma_{\min} \sim (V^c - V)$.

VI. CONCLUSION

We have presented a detailed analytical and numerical analysis of a viscoelastic model of friction in mean-field approximation, in which the driving velocity competes with the timescale of the viscoelastic effects within the system.

Our main findings are the following. At low driving velocities, we obtain a stick-slip dynamics with amplitudes of the stress oscillations that decrease with increasing driving velocity (V) or increasing driving stiffness (k_0). Beyond a

certain critical driving velocity ($V > V^c$), the amplitude of these oscillations becomes zero; i.e., the sliding is smooth. The transition between stick-slip and smooth-sliding occurs in a continuous manner and is very well described by a phenomenological rate-and-state analysis. In the smooth-sliding regime the friction force reduces as a function of the driving velocity, reproducing the well known velocity-weakening phenomenology. In our model, this effect is originated in the existence of viscoelastic elements that set an additional timescale for the dynamics. Finally, the response of our model to intermittent driving allowed us to reproduce qualitatively an important aspect of the aging of contacts, namely the increase of the static friction with time of contact at rest. Overall, we believe our model reproduces many well-known features of real tribology and gives a well-defined model on which many assumptions and predictions of phenomenological theories (like rate-and-state equations) can be investigated in depth.

ACKNOWLEDGMENTS

E.A.J. is financially supported by CONICET (Argentina). Partial support through Grant No. PICT 2012-3032 (ANPCyT, Argentina) is also acknowledged. We acknowledge the support by the France-Argentina MINCYT-ECOS Grant No. A12E05.

APPENDIX A: DETAILED DERIVATION OF THE EQUATIONS OF MOTION

We first study the one-dimensional case, as presented in Fig. 9.

The interface is decomposed in blocks of mass m, labeled i and moving along horizontal rails h_i. The action of the dashpot is to resist the change in $\phi_i - h_i$ via viscous friction, with a resulting force on h_i given by $\eta_u \partial_t(\phi_i - h_i)$. The blocks move in a medium with some effective viscosity η and we study the overdamped regime, $m\partial_t^2 h_i \ll \eta \partial_t h_i$. As each block is described by two degrees of freedom h_i and ϕ_i, the time evolution is governed by two equations. We now provide a pedestrian derivation of the equations, for the sake of completeness. The first equation comes from the force balance on h_i:

$$\eta\partial_t h_i = f_i^{\rm dis}(h_i) + k_0(w - h_i) + k_1(h_{i+1} - h_i) + k_1(h_{i-1} - h_i) + \eta_u\partial_t(\phi_i - h_i) + k_2(\phi_{i-1} - h_i). \tag{A1}$$

The second equation is derived from the force balance on ϕ_i:

$$0 = k_2(h_{i+1} - \phi_i) + \eta_u\partial_t(h_i - \phi_i), \tag{A2}$$

where we assume that the internal degree of freedom ϕ_i has no mass. Similarly, the force balance on ϕ_{i-1} yields

$$0 = k_2(h_i - \phi_{i-1}) + \eta_u\partial_t(h_{i-1} - \phi_{i-1}). \tag{A3}$$

In order to let the Laplacian term $k_2(h_{i+1} - 2h_i + h_{i-1})$ appear, we introduce the variable

$$u_i \equiv \phi_i - h_i + h_{i-1} - \phi_{i-1}, \tag{A4}$$

which represents the elongation of the dashpot elements connected to site i. We inject Eq. (A2) into Eq. (A1) to get rid of the time derivatives, and we subtract Eq. (A3) from Eq. (A2)

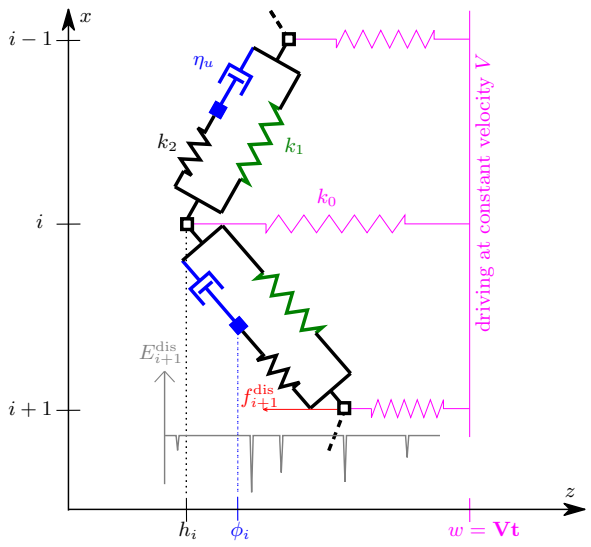

FIG. 9. (Color online) Sketch of the one-dimensional viscoelastic interface model. The interface itself (bold black line) consists in blocks set at discrete lattice sites $i, i+1, \ldots$ along the x axis (in higher dimensions, $x \in \mathbb{R}^d$). The blocks can evolve along the z axis: they are identified by their locations $h_i, h_{i+1}, \ldots$ (empty squares) and bound together via a combination of springs (k_1, k_2) and dashpots (η_u). The viscoelastic interaction introduces an internal degree of freedom ϕ_i, represented by full squares (blue). Driving is performed via springs k_0 linked to the position $w = Vt$ (thin purple lines). The disorder force $f_i^{\rm dis}$ (red) for the site i derives from a disordered energy potential $E_i^{\rm dis}(z)$ (gray).

to obtain Eq. (A6):

$$\eta\partial_t h_i = f_i^{\rm dis}(h_i) + k_0(w - h_i) + (k_1 + k_2)(h_{i+1} - 2h_i + h_{i-1}) - k_2 u_i, \tag{A5}$$

$$\eta_u\partial_t u_i = k_2(h_{i+1} - 2h_i + h_{i-1}) - k_2 u_i. \tag{A6}$$

A more elegant notation using the Laplacian operator ∇^2 is

$$\eta\partial_t h_i = f_i^{\rm dis}(h_i) + k_0(w - h_i) + k_1\nabla_i^2 h_i + k_2\big(\nabla_i^2 h_i - u_i\big),$$
$$\eta_u\partial_t u_i = k_2\big(\nabla_i^2 h_i - u_i\big). \tag{A7}$$

To generalize this to higher dimensions (on a square lattice), one simply has to connect each block h_i to its neighbors via viscoelastic elements, using a single orientation per direction. The equations obtained are exactly Eq. (A7) if we reinterpret the label i as referring to d-dimensional space, the Laplacian ∇^2 as the d-dimensional one, and the u_i variable as

$$u_i = \sum_{j=1}^{d}(\phi_j - h_j) + \sum_{j'=d+1}^{2d}(h_{j'} - \phi_{j'}), \tag{A8}$$

where indices j denote the d first neighbors, connected via a dashpot followed by the spring k_2 (and k_1 in parallel) and indices j' denote the last d neighbors, connected via the spring k_2 followed by a dashpot (and k_1 in parallel).

We study the mean-field limit via the fully connected approximation. In practice, each block position h_i interacts with the positions of all other blocks via $N - 1$ springs of elastic constant k_1/N (N being the number of blocks in the

system) and via $N-1$ viscoelastic elements (i.e., spring in series with a dashpot). As usual for fully connected systems, the final equation for the site i is obtained by replacing any occurrence of Δh_i with $\overline{h}-h_i$.

APPENDIX B: THE NUMERICAL METHODS

In previous works [8,35] we showed how to translate the stochastic dynamics into a master equation (or Fokker-Planck equation), but only in the case in which $V \to 0$. Here we generalize the procedure to any velocity V. Our Cython code is fully available [36].

It is useful to describe the dynamics using the local variable, δ_i:

$$\delta_i \equiv 1 - k_0(w-h_i) - (k_1+k_2)(\overline{h}-h_i) + k_2 u_i, \qquad \text{(B1)}$$

which represents the amount of additional stress that a site can hold before becoming unstable: as long as $\delta_i > 0, \forall i$, the block is stable and its position, h_i, remains fixed when $\delta_i = 0$ the block jumps to the next pinning well at a random distance z: $h_i \to h_i + z$. To define the dynamics in terms of δ variables, we need to split it in a *fast* part δ^F and a *relaxed* one δ^R:

$$\begin{aligned} \delta_i^F &= 1 - k_0(w-h_i) - (k_1+k_2)(\overline{h}-h_i), \\ \delta_i^R &= k_2 u_i, \end{aligned} \qquad \text{(B2)}$$

such that $\delta_i = \delta_i^F + \delta_i^R$. The blocks dynamics is controlled by three processes:

(i) *The avalanches.* When a block is unstable ($\delta_i \leqslant 0$), it moves to the next pinning wells: $\delta_i^F \mapsto \delta_i^F + z(k_0+k_1)$, with z drawn from $g(z)$. Each jump z is followed by a stress redistribution $\delta_j^F \mapsto \delta_j^F - zk_1/N$. These drops can trigger other instabilities. The characteristic duration of such an avalanche is $\tau_0 = \eta_0/\max(k_0,k_1,k_2)$.

(ii) *The driving.* External driving increases over time: for instance $w = Vt$ in the uniform driving protocol. In terms of δ, driving means that over a time step dt, $\delta_i^F \mapsto \delta_i^F - k_0 V dt$. This driving can happen until a new instability is triggered [step (i)]. The characteristic time scale of driving is $\tau_D = \overline{z}/V$.

(iii) *The relaxation.* In absence of instabilities, the h_i's are constant, and Eq. (2) reduces to

$$\delta_i^R(t) = k_2(\overline{h}-h_i) + \left[\delta_i^R(t_0) - k_2(\overline{h}-h_i)\right] e^{-k_2 \frac{t-t_0}{\eta_u}}, \qquad \text{(B3)}$$

where t_0 is the time at which the last avalanche occurred. Note that h_i does not evolve during relaxation or driving, so that relaxation can happen until a new instability is triggered [step (i)]. The characteristic time scale of relaxation is $\tau_u = \eta_u/k_2$.

In this paper we study the case $\tau_0 \ll \tau_u \sim \tau_D$ and focus on the case of the mean-field model where fluctuations vanish and the description of the system via a simple probability distribution becomes exact. Indeed, the sole distribution $P(\delta)$ does not provide enough information to fully characterize the system and its evolution. We consider the joint probability density distribution $P(\delta^F,\delta^R)$. The quantity $P(\delta^F,\delta^R,t)d\delta^F d\delta^R$ represents the probability for a site drawn at random to have a particular set of values of δ^F,δ^R and can be computed numerically starting from the dynamical rules that apply to the δ's.

To be concrete, we discretize $P(\delta^F,\delta^R)$ with a bin ε. The distribution probability is then a matrix $P_{i,j}$, where $P(\delta^F = \varepsilon i, \delta^R = \varepsilon j) d\delta^F d\delta^R = P_{i,j}$. We use a time step $dt = \varepsilon/k_0 V$ and define the constant $\kappa = k_0 + k_1 + k_2$.

The finite velocity is expressed through the fact that every time there is some driving of w by a quantity $dw = V dt$, there is also relaxation during a time dt. In particular, we define the relaxation factor $R(dt) = 1 - e^{-dtk_2/\eta_u}$. For the avalanches, two crucial quantities should be defined: (1) the fraction of unstable sites $P_{\text{unst}}^{\text{tot}} \equiv \varepsilon \sum_{i,j|i+j<0} P_{i,j} = \varepsilon \sum_j \sum_{i'|(i'+j<0)} P_{i',j}$, and (2) the stress redistribution $P_{\text{unst}}^{\text{tot}} \overline{z}(k_1+k_2)$ that follows the stabilization of the unstable sites. When $P_{\text{unst}}^{\text{tot}} \overline{z}(k_1+k_2) > 1$, the avalanche increases geometrically over the time steps, which is why it is practical to define a "critical" value $P_0^c = \frac{1}{\overline{z}(k_1+k_2)}$.

The sketch of the algorithm is the following.

(1) *Relaxation process*:

(i) Compute $j_\infty(i)$, the bin associated to the fully relaxed state, $\delta_{i,\infty}^R = \frac{k_2}{\kappa}(\overline{\delta^F} - \delta^F)$:

$$j_\infty(i) = \text{Int}\left[k_2 \frac{-i + \sum_{i',j} i' P(i',j)}{\kappa} \right].$$

(ii) Relaxation corresponds to shift[1] $P_{i,j}$ to $P_{i,j+\text{Shift}}$ (where $\text{Shift} = \text{Int}\{[j_\infty(i) - j]R(dt)\}$), set $r = 1$ and perform the *Avalanche process*.

(2) *Avalanche process*: consists of driving and jumps.

(i) Driving:

$$P_{i,j} \leftarrow P_{i,j} + (P_{i+1,j} - P_{i,j}) r. \qquad \text{(B4)}$$

(ii) Compute $P_{\text{unst}}(j) = \sum_{i'|i'+j<0} P_{i',j}$.

(iii) Jumps:

$$\begin{aligned} P_{i,j} &\leftarrow P_{i,j} + \frac{\varepsilon}{\kappa} g\left(\frac{\varepsilon(i+j)}{\kappa}\right) P_{\text{unst}}(j), \\ P_{i,j} &\leftarrow 0 \quad \text{if } i+j<0. \end{aligned} \qquad \text{(B5)}$$

(iv) Compute $P_0 = \sum_{i=-j} P_{i,j}$.

(v) If $P_0 \geqslant P_0^c$, set $r = 1$ and perform the *Avalanche process* again.

(vi) Else

(a) Compute $P_{\text{unst}}^{\text{tot}} = \sum_j P_{\text{unst}}(j)$.

(b) If $P_{\text{unst}}^{\text{tot}} \geqslant P_0^c/100$, set $r = \min(1, P_{\text{unst}}^{\text{tot}}/P_0^c)$ and perform the *Avalanche process* again.

(c) Else, perform the *Relaxation process*.

Here we used the exponential distribution with $\overline{z} = 0.2$ and an upper-length cutoff $g(z) = 1/\overline{z} e^{-z/\overline{z}} \Theta(z)\Theta(10-z)$, where Θ is the Heaviside function. We always used $\eta_u = 1$.

Above V^c we consider that the stationary regime is reached when the relative variation between the last three values of σ does not exceed 1%. Below V^c we ask that the stress drops $\Delta\sigma$ of three consecutive global shocks change less than 1%. Finally, the critical value V^c is found by decimation: starting with a very small $V_{\min} = 1e^{-4}$ and very large $V_{\max} = 1000$, simulations are repeated between the two boundaries until the relative difference between those two boundaries is less than

[1] Instead of crudely taking the integer part of $[j_\infty(i) - j]R(dt)$, it is numerically much more stable to split the shift over the two bins, using a linear interpolation.

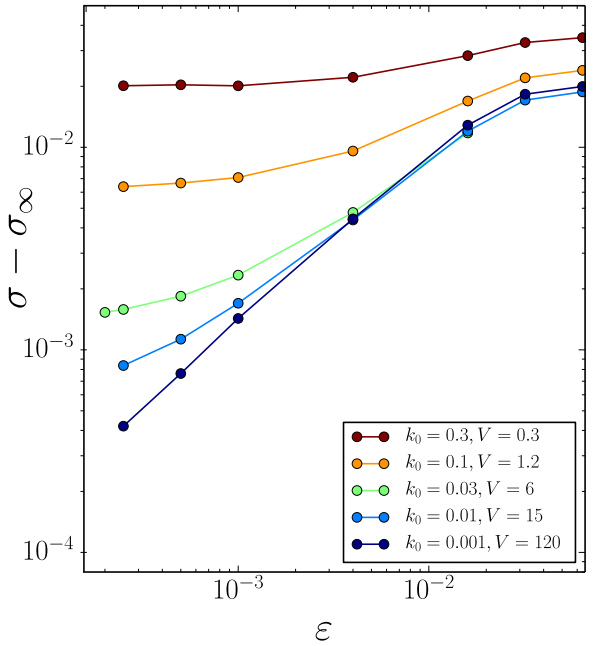

FIG. 10. (Color online) Convergence of the stress to its limit value $\sigma(V)$, as the binning ε decreases. We selected velocities V close to but larger than V^c for the five values of k_0 studied (from top to bottom: decreasing k_0 and increasing V). Convergence is reached for the three largest values of k_0.

1%. This means that a larger absolute tolerance is allowed for larger values of V^c.

An issue limiting higher precision is the presence of numerical instabilities when approaching to the critical point. In Fig. 10 the dependence of σ on the binning ε is shown. For large values of k_0 (0.3, 0.1, and 0.03), it is clear that we converge toward a plateau $\sigma(V)$ when the binning decreases. The small values of k_0 represent a challenge, because the precision required from the algorithm is $\sim\bar{z}k_0$. However, comparing the expected values (dashed lines) and the behavior at larger k_0's, it can be expected that smaller binnings would produce the expected results.

APPENDIX C: ANALYTICAL SOLUTION FOR THE STATIONARY REGIME

Let us now solve the model of Fig. 2(b). We call $f^0(t)$, $f^1(t)$, and $f^2(t)$ the forces coming from the branches with the k_0, k_1, and k_2 springs. The coordinate h_i will jump to $h_i + \bar{z}$ each time

$$f^0(t) + f^1(t) + f^2(t) = f^{\text{th}}. \tag{C1}$$

Between jumps, the different forces behave as

$$f^0(t) = f_a^0 + k_1 V t, \tag{C2}$$

$$f^1(t) = f_a^1 + k_0 V t, \tag{C3}$$

$$f^2(t) = V\eta + \left(f_a^2 - V\eta_u\right)\exp\left(-\frac{k_2 t}{\eta_u}\right), \tag{C4}$$

where the a subindexes on the right indicate values of the forces right after the jump. This expression holds until the next jump that occurs at time $t \equiv \bar{z}/V$. At this moment, the forces must satisfy Eq. (C1), and we obtain

$$f_b^0 = f_a^0 + k_1\bar{z}, \tag{C5}$$

$$f_b^1 = f_a^1 + k_0\bar{z}, \tag{C6}$$

$$f_b^2 = V\eta + \left(f_a^2 - V\eta_u\right)\exp\left(-\frac{k_2\bar{z}}{V\eta_u}\right), \tag{C7}$$

where the b subindex stands for the values right before the jump. In addition, we have $f_b^1 = -f_a^1$ since the average value of f^1 must vanish. Also, since the dashpot is rigid at the jump, we get $f_b^2 - f_a^2 = \bar{z}k_2$. From all these equations all forces $(f_b^0, f_a^0, f_b^1, f_a^1, f_b^2, f_a^2)$ can be calculated. In particular we are interested in the average friction force σ which is given by $\sigma = (f_a^0 + f_b^0)/2$. Through a straightforward elimination procedure we get the Eq. (4) given in the main text.

[1] B. N. J. Persson, U. Tartaglino, O. Albohr, and E. Tosatti, Rubber friction on wet and dry road surfaces: The sealing effect, Phys. Rev. B **71**, 035428 (2005).
[2] B. N. J. Persson, Rubber friction and tire dynamics, J. Phys. Condensed Matter: Inst. Phys. J. **23**, 015003 (2011).
[3] J. H. Smith and J. Woodhouse, The tribology of rosin, J. Mech. Phys. Solids **48**, 1633 (2000).
[4] S. Serafin, C. Vergez, and X. Rodet, Friction and application to real-time physical modeling of a violin, Proceedings of the International Computer Music Conference (ICMC) Beijing, China (1999), https://hal.archives-ouvertes.fr/hal-01105504.
[5] D. W. Lee, X. Banquy, and J. N. Israelachvili, Stick-slip friction and wear of articular joints, Proc. Natl. Acad. Sci. U.S.A. **110**, E567 (2013).
[6] T. Baumberger, C. Caroli, B. Perrin, and O. Ronsin, Nonlinear analysis of the stick-slip bifurcation in the creep-controlled regime of dry friction, Phys. Rev. E **51**, 4005 (1995).
[7] T. Baumberger and C. Caroli, Solid friction from stick-slip down to pinning and aging, Adv. Phys. **55**, 279 (2006).
[8] E. A. Jagla, F. P. Landes, and A. Rosso, Viscoelastic effects in avalanche dynamics: A key to earthquake statistics, Phys. Rev. Lett. **112**, 174301 (2014).
[9] M. Radiguet, D. S. Kammer, and J. F. Molinari, The role of viscoelasticity on heterogeneous stress fields at frictional interfaces, Mech. Materials **80**, 276 (2015).
[10] M. Di Bartolomeo, F. Massi, L. Baillet, A. Culla, A. Fregolent, and Y. Berthier, Wave and rupture propagation at frictional bimaterial sliding interfaces: From local to global dynamics, from stick-slip to continuous sliding, Tribol. Int. **52**, 117 (2012).
[11] D. S. Amundsen, J. Scheibert, K. Thøgersen, J. Trømborg, and A. Malthe-Sørenssen, 1D model of precursors to frictional stick-slip motion allowing for robust comparison with experiments, Tribol. Lett. **45**, 357 (2012).
[12] M. Kardar, Nonequilibrium dynamics of interfaces and lines, Phys. Rep. **301**, 85 (1998).

[13] D. S. Fisher, Collective transport in random media: From superconductors to earthquakes, Phys. Rep. **301**, 113 (1998).
[14] J. P. Sethna, K. A. Dahmen, and C. R. Myers, Crackling noise, Nature **410**, 242 (2001).
[15] S. Zapperi, P. Cizeau, G. Durin, and H. E. Stanley, Dynamics of a ferromagnetic domain wall: Avalanches, depinning transition, and the Barkhausen effect, Phys. Rev. B **58**, 6353 (1998).
[16] A. Rosso, Depiegeage de variétés élastiques en milieu aléatoire, Ph.D. thesis, Université Pierre et Marie Curie-Paris VI, 2002.
[17] J. M. Schwarz and D. S. Fisher, Depinning with dynamic stress overshoots: A hybrid of critical and pseudohysteretic behavior, Phys. Rev. E **67**, 021603 (2003).
[18] M. C. Marchetti, A. A. Middleton, and T. Prellberg, Viscoelastic depinning of driven systems: Mean-field plastic scallops, Phys. Rev. Lett. **85**, 1104 (2000).
[19] M. C. Marchetti, Models of plastic depinning of driven disordered systems, Pramana **64**, 1097 (2005).
[20] E. A. Jagla and A. B. Kolton, A mechanism for spatial and temporal earthquake clustering, J. Geophys. Res. **115**, B05312 (2010).
[21] E. A. Jagla, Realistic spatial and temporal earthquake distributions in a modified Olami-Feder-Christensen model, Phys. Rev. E **81**, 046117 (2010).
[22] M. Bottiglieri, L. de Arcangelis, C. Godano, and E. Lippiello, Multiple-time scaling and universal behavior of the earthquake interevent time distribution, Phys. Rev. Lett. **104**, 158501 (2010).
[23] L. E. Aragón, E. A. Jagla, and A. Rosso, Seismic cycles, size of the largest events, and the avalanche size distribution in a model of seismicity, Phys. Rev. E **85**, 046112 (2012).
[24] S. Papanikolaou, D. M. Dimiduk, W. Choi, J. P. Sethna, M. D. Uchic, C. F. Woodward, and S. Zapperi, (SI) Quasi-periodic events in crystal plasticity and the self-organized avalanche oscillator, Nature **490**, 517 (2012).
[25] B. D. Kilgore, M. L. Blanpied, and J. H. Dieterich, Velocity dependent friction of granite over a wide range of conditions, Geophys. Res. Lett. **20**, 903 (1993).
[26] J. H. Dieterich, Modeling of rock friction: 1. Experimental results and constitutive equations, J. Geophys. Res. **84**, 2161 (1979).
[27] A. Ruina, Slip instability and state variable friction laws, J. Geophys. Res. **88**, 10359 (1983).
[28] A. Dobrinevski, P. Le Doussal, and K. J. Wiese, Statistics of avalanches with relaxation and Barkhausen noise: A solvable model, Phys. Rev. E **88**, 032106 (2013).
[29] R. Capozza, I. Barel, and M. Urbakh, Probing and tuning frictional aging at the nanoscale, Sci. Rep. **3**, 1896 (2013).
[30] C. H. Scholz, *The Mechanics of Earthquakes and Faulting* (Cambridge University Press, Cambridge, 2002).
[31] A. Vanossi, N. Manini, M. Urbakh, S. Zapperi, and E. Tosatti, Colloquium: Modeling friction: From nanoscale to mesoscale, Rev. Modern Phys. **85**, 529 (2013).
[32] J. Krim, Resource Letter: FMMLS-1: Friction at macroscopic and microscopic length scales, Am. J. Phys. **70**, 890 (2002).
[33] K. Thøgersen, J. r. K. Trømborg, H. A. Sveinsson, A. Malthe-Sørenssen, and J. Scheibert, History-dependent friction and slow slip from time-dependent microscopic junction laws studied in a statistical framework, Phys. Rev. E **89**, 052401 (2014).
[34] Y. Bar-Sinai, R. Spatschek, E. A. Brener, and E. Bouchbinder, On the velocity-strengthening behavior of dry friction, J. Geophys. Res.: Solid Earth **119**, 1738 (2014).
[35] F. P. Landes, Viscoelastic Interfaces Driven in Disordered Media and Applications to Friction, Ph.D. thesis, Université Paris-Sud, Orsay, 2014 (Springer Theses).
[36] Git Repository (2014), https://bitbucket.org/flandes/viscoelastic_meanfield_fokkerplanck/.